SCIENCE CHINA
Technological Sciences

•Article•

October 2021 Vol.64 No.10: 2174–2185
https://doi.org/10.1007/s11431-021-1881-8

Uncertainty analysis and robust design optimization for the heat-assisted bending of high-strength titanium tube

ZHANG Zhao[1,2], YANG JingChao[1,2], HUANG WeiLiang[1,2], MA Jun[1,2] & LI Heng[1,2*]

[1] *Taicang Yangtze River Delta Research Institute, Northwestern Polytechnical University, Taicang 215400, China;*
[2] *State Key Laboratory of Solidification Processing, Northwestern Polytechnical University, Xi'an 710072, China*

Received March 16, 2021; accepted June 23, 2021; published online September 3, 2021

Heat-assisted rotary draw bending (HRDB) is a promising technique for manufacturing difficult-to-form tubular components comprising high-strength titanium tubes (HSTTs) with small bending radii. However, as a multidie constrained and thermomechanical coupled process with many uncertainty factors, a high risk of several defects, such as cross-section distortion, over wall thinning, or even cracking, is present. Achieving the robust design optimization (RDO) of complex forming processes remains a nontrivial and challenging scientific issue. Herein, considering a high-strength Ti-3Al-2.5V titanium alloy tube as a case material, the five significant uncertainty factors in HRDB, i.e., temperature distribution, tube geometrical characteristics, tube material parameters, tube/tool friction, and boost velocity had been analyzed. Subsequently, considering the preheating and HRDB of HSTT, a whole-process thermomechanical three-dimensional finite element model was established and validated for virtual experiments. Further, considering the maximum section distortion Q and maximum wall-thickness thinning t as the optimization objectives and the mean and variance of material and forming parameters, an RDO model was established. Finally, the Pareto optimal solutions were obtained using the nondominated sorting genetic algorithm II, and a minimum distance selection method was employed to obtain the satisfactory solution. Results show that the optimized solutions considering the uncertainty factors reduce the maximum section distortion rate of HSTT after bending by 38.1% and the maximum wall-thickness thinning rate by 27.8%.

robust design optimization, uncertainty factors, heat-assisted bending, high-strength titanium tube

Citation: Zhang Z, Yang J C, Huang W L, et al. Uncertainty analysis and robust design optimization for the heat-assisted bending of high-strength titanium tube. Sci China Tech Sci, 2021, 64: 2174–2185, https://doi.org/10.1007/s11431-021-1881-8

1 Introduction

High-strength titanium tubes (HSTTs) are characterized by high-pressure resistance, high reliability, and long lifetime; thus, they have been widely used in the aviation and aerospace industries. Compared with aluminum alloy and stainless tubes, HSTTs are difficult-to-form tubular materials with high strength, low hardening exponent, and poor ductility at room temperature [1]. During bending, especially when the bending radius is small, severe tube nonuniform deformation may cause multiple defects, such as overthinning, fracture, overflattening, and convex hull [2]. Figure 1 shows the common defects during the bending process. Heating high-strength titanium alloy to temperatures below the recrystallization temperature not only reduces deformation resistance and improves the formability of tube materials but also prevents the phase transformation, dynamic recrystallization, high cost, and energy consumption of high-temperature forming. Thus, incorporating heating into the universal bending process, heat-assisted rotary draw bending (HRDB) is expected to break the bending limit of HSTT. However, as a complex nonlinear process involving multidie constrained and thermomechanical coupled effects, HRDB easily induces several defects, such as cross-sectional dis-

*Corresponding author (email: liheng@nwpu.edu.cn)

Figure 1 (Color online) Defects in the bending of a high-strength Ti-3Al-2.5V tube with a small bending radius.

tortion, over wall thinning, or even cracking. Various uncertainty factors exist during the whole process, such as temperature distribution, tube geometrical characteristics, tube material parameters, tube/tool friction, and boost velocity. Therefore, robust design optimization (RDO) is expected to improve the stability of forming quality and reduce the sensitivity of forming results to fluctuations of uncertainty factors. However, it is still challenging to achieve accurate and efficient control of the forming process under multiple objects, constraints, and uncertainty factors.

In the past two decades, the heat-assisted bending of difficult-to-form tubular materials and structures has been investigated. Hao and Li [3] established an analytical model to describe the bending angle in laser bending to determine the relationship between bending angles and machining parameters. Guan et al. [4] established a three-dimensional (3D) thermomechanical finite element (FE) model of stainless steel laser bending and found that the number of scans is proportional to the bending angle. Hu [5] established an FE model for the local induction-heating bending of tubes with a small bending radius (R/D=1.5). Collie et al. [6] predicted the geometric shape of deformed tubes by establishing an elastic-plastic FE model and found that large-diameter steel-tube forming is difficult when a tube is heated to bend with a small bending radius (R/D=1.5). Huang and Lu [7] studied the influence of hot-push bending mandrel design on the size and shape of tubes. Considering nonuniform local heating and multidie constraints, Tao et al. [8] established a whole-process thermomechanical coupling 3D FE model of large-diameter thin-walled Ti-6Al-4V tube warm bending based on ABAQUS. Simonetto et al. [9] established a numerical model of induction-heating bending and studied the influence of different heating strategies and process temperature on the forming process. They revealed the risk of defects. Zhang et al. [10] established a 3D FE heat-assisted bending model and simulated the influence of preheating temperature on the temperature distribution of bending dies and thickness of tube walls. Most of the cited studies focus on the heat-assisted bending numerical simulation of tubular materials, and the design optimization of the bending process has rarely been reported. Moreover, these studies did not consider the RDO regarding uncertainty factors in bending forming.

RDO renders the product quality insensitive to the influence of design parameters and noise factors, and it has been widely used in metal forming [11]. In RDO, the insensitivity of the objective function is emphasized, and the weighted summation formula is combined with the minimized objective function. Moreover, RDO is not sensitive to model errors, and random input data can be insufficient; therefore, it is more effective than other methods. Using the Monte Carlo sampling, response surface method, and most probable point method, the uncertainty in the near-net forming of sheet metals, blade forging, and forward extrusion of axisymmetric members have been analyzed, and the robust design has been developed [12]. Huang et al. [13] established the double-response surface model of T-tube hydroforming, and the robust Pareto optimal solution was obtained using the nondominated sorting genetic algorithm II (NSGA-II) and ideal point method. Chen et al. [14] established a robust design model for controlling wall thinning by simulating the bending process and calculating the value of the objective function. The optimal design parameters were obtained, and the wall-thickness reduction was effectively controlled. Strano [15] considered the influence of uncertainty factors in sheet metal forming, minimizing the cost function established using the approximate model, and proposed a four-step stochastic optimization method for metal forming optimization. Sun et al. [16] proposed a multiobjective robust optimization method to solve the influence of parameter uncertainty on draw bead design. Yin et al. [17] proposed a multiobjective robust optimization method to improve the crashworthiness of tapered thin-walled tubes, combining the kriging element model and multiobjective particle swarm optimization algorithm to obtain the Pareto frontier optimal solution. However, achieving RDO in complex forming processes remains a nontrivial and challenging scientific issue. The above studies provide references for the RDO of the heat-assisted bending process for high-strength titanium alloy tubular materials.

Considering Ti-3Al-2.5V HSTT as a case material and uncertainty factors in HRDB, herein, this study investigates the RDO for the thermal-mechanical coupled forming process. First, the forming indexes of the HRDB of HSTT were identified, the source of the uncertainty of forming parameters in the HRDB of HSTT was analyzed, the fluctuation range of the uncertainty factors was determined, and the significance of the uncertainty was analyzed. Second, the RDO mathematical model of the HRDB of HSTT was es-

tablished, inside and outside an array orthogonal design was constructed using the Box-Behnken design (BBD) and uniform design (UD), and mean value and variance of the forming indexes were calculated using a 3D FE model for constructing the response surface model (RSM). Furthermore, the Pareto optimal solutions were obtained using NSGA-II, and the minimum distance selection method was employed to determine the satisfactory solution from the Pareto optimal solutions. Finally, the effectiveness and robustness of the optimization results were verified experimentally.

2 Heat-assisted bending and source of uncertaintyfactors

2.1 Characteristics of HRDB and forming a quality index

HRDB dies mainly include bend, insert, clamp, wiper, and pressure dies, and mandrel (with multiple flexible balls), as shown in Figure 2 [15]. The bend die has a fixed bending radius and is the main forming die of bending. The insert and clamp die press the tube on the bend die and draw it, rotating along with the bend die. The pressure die is used to bend and compact the tube, working with the wiper die to prevent wrinkling and promote the stable forming of the tube. The mandrel with flexible balls supports the inner side of the tube to prevent wrinkling and cross-section distortion. As shown in Figure 2(b), the heating and thermometer holes are opened toward dies (such as pressure and wiper dies), and the dies are heated by the resistance rods in the temperature control system. Finally, the heat is transferred to the tube. After the bending-zone temperature reaches the target value, the bending process begins. Heat conduction in the dies and bending machine significantly reduces the heating efficiency, and a heat insulation board is added between the dies and bending machine. The low bending speed prevents sliding and excessive distortion in the clamping area. Because the heat capacity of the HSTT is small, the tube temperature during the bending process depends on the die temperature. Heating the pressure die and mandrel can reduce heat conduction from the bending and wiper dies to the bending machine and maintain the outside of the tube in a reasonable temperature range to improve the bend-forming potential.

Therefore, the HRDB process of HSTT comprises two subprocesses: die heating and tube heat-assisted bending. In the first process, the tube and dies are fully assembled, and the dies are heated using a resistance rod. The die temperature is recorded using a thermocouple, and the heating process is controlled via a temperature control system. After heating for a certain period, the temperature reaches a reasonable range, and HSTT is subjected to continuous local elastic-plastic deformation under the combined action of multidie constraint and nonuniform temperature field, and the numerical control (NC) HRDB begins. When the tube reaches the target bending angle, the mandrel is extracted and the die is unloaded; subsequently, the NC-HRDB forming of HSTT is completed.

A structure with a small diameter, thin wall, and small bending radius and tubular materials with the weak hardening effect and low toughness result in many defects, such as excessive section distortion and excessive wall thinning. Thus, the bending quality of HSTT can be represented using two indexes: the maximum section distortion Q and maximum outside wall-thickness thinning t.

$$Q = \frac{D_0 - D_{\min}}{D_0} \times 100\%, \tag{1}$$

where D_0 represents the original tube diameter, and $D_{\min}$ denotes the minimum section diameter.

$$t = \frac{t_0 - t_{\min}}{t_0} \times 100\%, \tag{2}$$

where t_0 represents the original tube wall thickness, and $t_{\min}$ denotes the minimum outside wall thickness after bending.

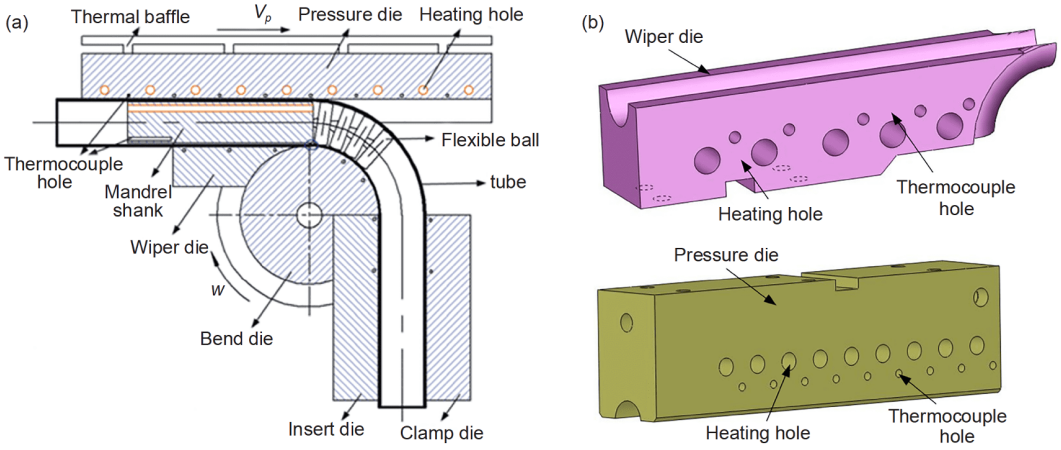

Figure 2 (Color online) Dies of HRDB. (a) Schematic of HRDB process [15]; (b) position of heating holes in wiper and pressure dies.

2.2 Selection of uncertainty factors

2.2.1 Fluctuation in temperature

An adequate heating temperature is one of the most important conditions for the NC-HRDB of HSTT. In the whole forming process, the temperature change of the tube and dies is complex. Thus, for the RDO of HRDB, accurately measuring the temperature of the tube and dies is important. However, directly measuring the temperature of the bending area of the tube is impossible, and the die temperature close to the tube reflects the tube temperature. Five and seven temperature measuring points are present in the wiper and pressure dies, respectively (Figure 3).

In the actual measurement process, the temperature is affected by friction, environmental temperature changes, improper filling of die insulation materials, variations in the output power of the heating rod, inaccurate temperature measurement, and delay in the feedback of the temperature control system, making the forming temperature different from the target value. As shown in Figure 4, the first and seventh temperature measuring points reflect the inside and outside temperatures of the tube, T_{inside} and T_{outside}, respectively, and T_{inside} and T_{outside} fluctuate in the range of 280°C–330°C. Figure 5 shows the simulation result of the temperature history of the NC-HRDB of HSTT. The position of the tube temperature points corresponds to the position of the die temperature measuring hole. A change in the inside temperature is reflected by recording the temperature history of the tube from the first to the fifth point (Figure 5(a)), and that of the outside temperature is reflected by recording the temperature history of the tube from the sixth to the tenth point (Figure 5(b)). The fluctuation in the inside temperature is lower than that of the outside temperature, and the temperature fluctuation range of the bending process is 285°C–332°C.

2.2.2 Fluctuation in tube geometrical characteristics

To determine the geometric fluctuation of HSTT, a vernier caliper with an accuracy of 0.01 mm was used to measure the tube diameter, and a spiral micrometer with an accuracy of 0.01 mm was used to measure the tube wall thickness. Ten samples with the same length were selected among the received material, and ten typical positions were selected in each sample. The diameter and wall thickness of 10 typical positions were measured, and the mean value was calculated (Tables 1 and 2). Table 1 lists the diameter fluctuation of HSTT and its mean value and standard deviation. The diameter of the HSTT varied between 19.98 and 20.10 mm; the mean value was 20.02 mm, standard deviation was 0.044, and fluctuation was 0.6%. Table 2 shows the wall thickness of HSTT and its mean value and standard deviation. The wall thickness of HSTT varied between 1.47 and 1.54 mm; the mean value was 1.502 mm, standard deviation was 0.019, and fluctuation was 4.67%.

2.2.3 Fluctuation in tube material parameters

Fluctuation in material parameters can cause instability in the forming quality in the process of the NC-HRDB of HSTT. The strong anisotropy evolution of plasticity in the TA18 thermomechanical process renders it difficult to control the forming quality [1]. In the tube bending process, with an increase in the contractile strain ratio (CSR) *R*-value, the thickness reduction in the outside wall of the tube decreases, whereas the tube section deformation degree increases correspondingly. Therefore, the variation in the *R*-value is a major influencing factor in the robust design. The variation in the *R*-value is shown in Figure 6. It varies between 2.05 and 2.51. The difference between the maximum and minimum *R*-values is 0.46. The variation in *R*-value is 19%, which is high.

2.2.4 Fluctuation of friction

In the actual bending forming process, the friction between the tube and dies influences the bending forming quality. The contact between the clamping die and tube and the pressure die and tube is dry friction, that between the bending die and

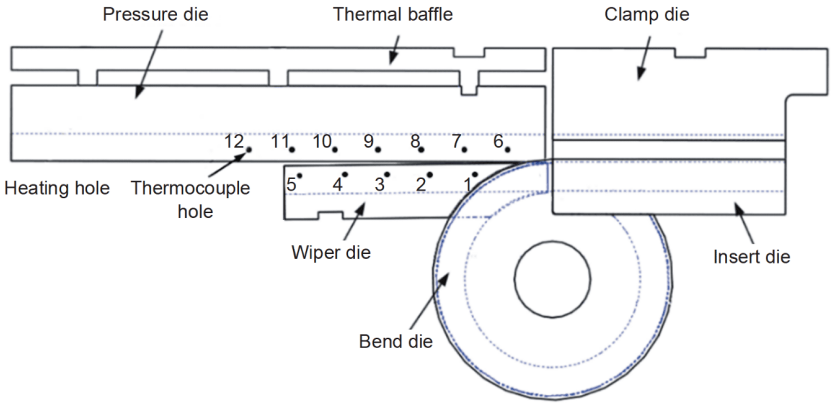

Figure 3 (Color online) Die temperature measurement positions.

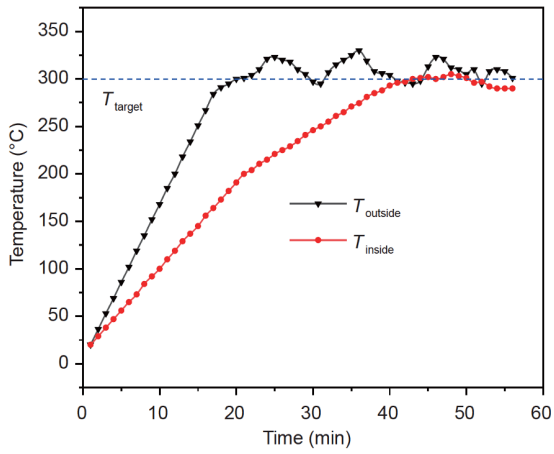

Figure 4 Temperature history of warm bending.

tube and the wiper die and tube is general lubrication, and that between the mandrel and tube is full lubrication. Under the states of the above contact type, the friction fluctuates within a certain range. The friction coefficient f_m influences the forming quality. The friction states affect the deformation and surface quality of the bending section. Further, the friction states affect the tube structure and life. In the bending process, the friction between the mandrel and tube should be as small as possible. In the current lubrication state, the frictional coefficient is 0.05–0.15.

2.2.5 Other random fluctuations

Due to the instability in the hydraulic transmission of bending machines, the boost speed of the pressure die fluctuates. The boost velocity greatly fluctuates in the early bending state and remains stable afterward. To avoid the influence of the boost velocity fluctuation on the forming quality, several empty bends should be made before bending to stabilize the hydraulic system and adjust the boost velocity. After many bending experiments, random fluctuations such as die wear, a shift in the die installation positions, a failure of mechanical equipment, and environmental temperature change also affect the forming quality. Although quantitatively describing these fluctuations in the actual bending process is difficult, random fluctuations should be avoided to reduce their impact on the forming quality.

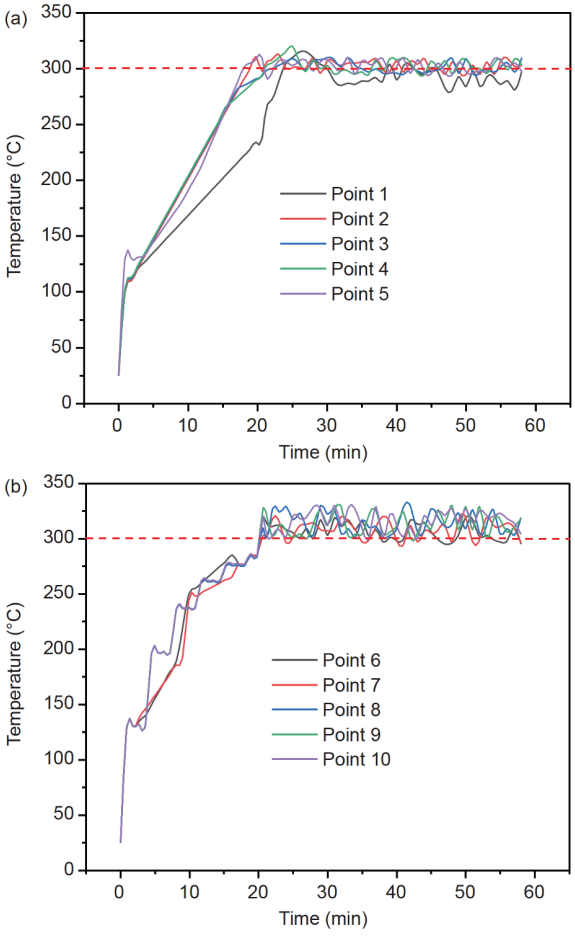

Figure 5 Simulated temperature history of warm bending. (a) Inside; (b) outside.

3 RDO modeling for the HRDB of HSTT

3.1 Mathematical model of RDO

Eq. (3) expresses the multiobjective robust optimization model for the HRDB forming parameters of HSTT. The design variables include mandrel diameter d_m, mandrel

Table 1 Measurement of the diameter fluctuation of Ti-3Al-2.5V HSTT

Nominal diameter (mm)	Actual measuring diameter (mm)										μ (mm)	σ
	1	2	3	4	5	6	7	8	9	10		
20	20.08	20.07	20.10	19.95	20	20.01	20.02	20	20	19.99	20.02	0.044

Table 2 Measurement of the wall-thickness fluctuation of Ti-3Al-2.5V HSTT

Nominal thickness (mm)	Actual measuring thickness (mm)										μ (mm)	σ
	1	2	3	4	5	6	7	8	9	10		
1.5	1.54	1.50	1.49	1.48	1.50	1.47	1.50	1.51	1.52	1.51	1.502	0.019

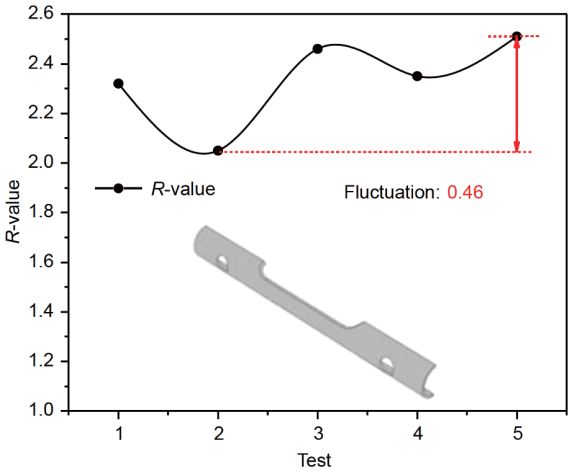

Figure 6 (Color online) Measurement results of *R*-value fluctuation.

elongation e, and boost coefficient K_{vp}. The objectives of robust optimization are the minimal sum of the mean and variance of the maximum cross-section distortion rate Q, and the maximum wall-thickness thinning rate t, and finally, to obtain the optimal solution of the forming parameters.

$$\begin{cases} \text{Variables: } d_m,\ e,\ K_{vp}, \\ \text{Minimum: } (Q^{\mu}+Q^{\sigma},\ t^{\mu}+t^{\sigma}), \\ \text{Constraint: } Q-5\% \le 0,\ t-20\% \le 0, \\ \text{Within ranges:} \\ \qquad 16.42 \le d_m \le 16.82,\ 0 \le e \le 2, \\ \qquad 1 \le K_{vp} \le 1.2. \end{cases} \tag{3}$$

3.2 3D FE modeling for HRDB for virtual experiments

According to the multidie constrained and local heating of the HRDB process, a 3D FE model for the HRDB process was developed using ABAQUS, which includes the pre-heating and heat-assisted bending models.

In the heating model, the 3D solid model simulates the actual heating process. The tube and dies with regular structure use DC3D8 element, and the irregular structure uses DC3D4 to improve computing efficiency. Considering heating combination, heating the pressure and wiper dies simultaneously and arranging the resistance heating rod along the axial direction of the pressure die can improve the heating efficiency, average temperature, and temperature uniformity of the tube and dies. The static implicit solver ABAQUS/Standard was adopted to simulate the heating process.

In the bending model, the dies are simplified to a rigid body, the tube is defined as a 3D elastoplastic deformable body, and the semitube model is chosen to improve the simulation accuracy and reduce the simulation time. The local refined meshing techniques are applied to avoid the meshing-induced singularity. The bending deformation area of the tube is divided into smaller meshes, whereas the straight section is divided into larger meshes. Moreover, the tube material model adopts the Hill48'R material constitutive model, and the contact surfaces between the tube and dies are simplified into face-to-face contact. The geometric model and temperature distribution at the dies and tube of the heating and bending stages are shown in Figure 7.

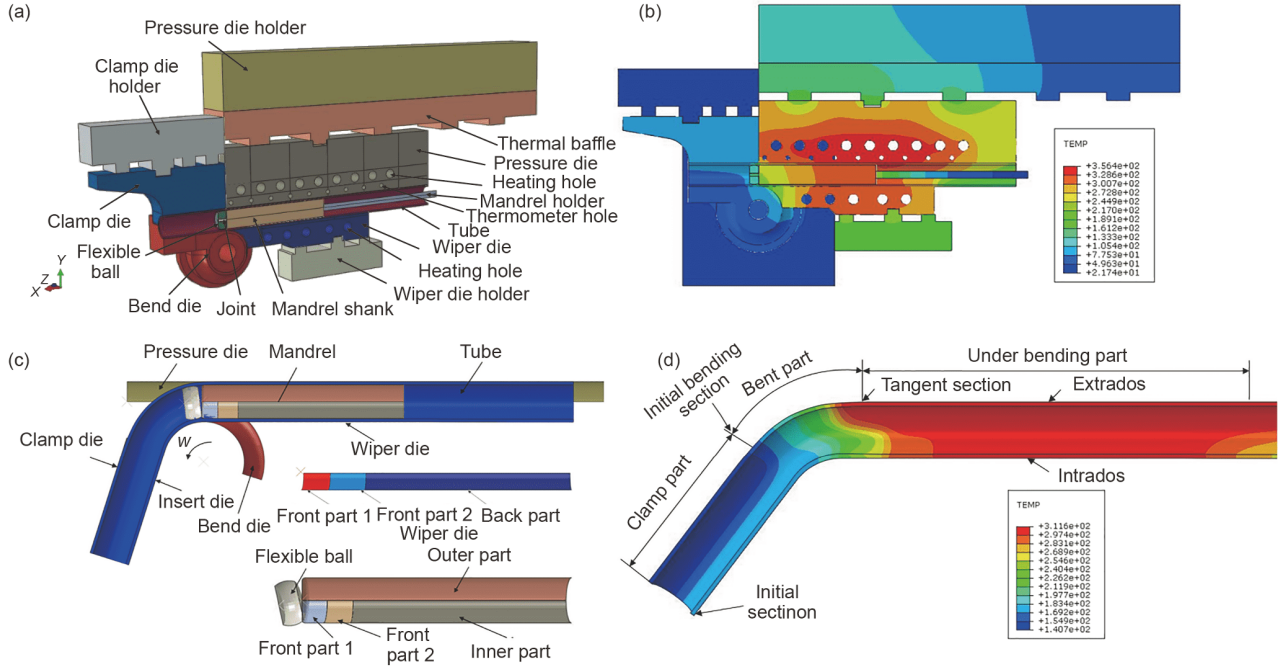

Figure 7 (Color online) Simulation of heating and bending stages during the HRDB of HSTT. (a) Geometric model of dies; (b) temperature distribution of dies in the heating stage; (c) geometric model of the bending stage; (d) temperature distribution of tube in the bending stage.

4 Results and discussion

4.1 Significance analysis of uncertainty factors

Herein, in the HRDB process of HSTT, the fluctuation in temperature T, geometric size (diameter D_0, wall thickness t_0), material parameter R, and friction coefficient f_m, are the uncertainty factors. To select the uncertainty factors that have little impact on the forming process and then reduce the number of tests to improve the efficiency of robust optimization design, the Plackett-Burman test was conducted to obtain the significance of the uncertainty factors. Two levels were selected for each uncertainty factor, and the total number of test groups is 12 (Tables 3 and 4). The response targets are the maximum cross-section distortion rate Q, and maximum wall-thickness thinning rate t.

The results of the significance analysis are shown in Figures 8 and 9. With an increase in T, f_m, and D_0, Q and t decrease, and the change in D_0 has the most significant effect on the forming quality. An increase in the R-value increases Q and t. The change in t has the least effect on the forming quality, so it can be eliminated. Based on the above analysis, the uncertainty factors D_0, T, f_m, and R have significant effects on Q and t, so their fluctuations should be considered in RDO.

4.2 Multiobjective robust optimization design

To consider the deterministic and uncertainty factors simultaneously, we employed the Taguchi method [18]. As listed in Table 5, the uncertainty factors are in the inner arrays, and the deterministic factors are in the outer arrays. Subsequently, the dual-RSMs of the target mean and variance that are affected by the uncertainty factors could be calculated, respectively. The test designs are shown in Tables 6 and 7. The uncertainty factors T, R, f_m, and D_0 are in the inner arrays, and the deterministic factors e, d_m, and K_{vp} are in the outer arrays. The response target Q and t are obtained using virtual experiments, the mean value and variance are calculated, and then, the dual-RSM is constructed.

According to the data of the test sample points in Table 6, the dual-RSM for the mean and variance of Q is established (eqs. (4) and (5)).

$$\begin{aligned} Q^{\mu} = {} & 4513.30308 - 540.04587 d_m + 5.02342 e \\ & - 36.82522 K_{vp} \\ & - 0.30625 d_m e + 16.24671 d_m^2 + 15.86184 K_{vp}^2, \end{aligned} \tag{4}$$

$$\begin{aligned} Q^{\sigma} = {} & 1473.10430 - 179.10612 d_m - 3.87869 e + 21.24584 K_{vp} \\ & + 0.22380 d_m e + 5.40103 d_m^2 + 0.061660 e^2 - 9.44712 K_{vp}^2. \end{aligned} \tag{5}$$

According to the data of test sample points in Table 7, the dual-RSM for the mean and variance of t is established (eqs. (6) and (7)).

$$\begin{aligned} t^{\mu} = {} & 9019.41196 - 1105.34222 d_m - 0.14313 e \\ & + 170.80208 K_{vp} \\ & - 10.72917 d_m K_{vp} + 33.92303 d_m^2, \end{aligned} \tag{6}$$

Table 3 Uncertainty factors and levels

Level	Uncertainty factors				
	T (°C)	f_m	R	D_0 (mm)	t_0 (mm)
−1	280	0.05	2	19.98	1.47
1	330	0.15	2.5	20.10	1.54

Table 4 Plackett-Burman test design scheme

No.	Uncertainty factors					Objectives	
	T (°C)	f_m	R	D_0 (mm)	t_0 (mm)	Q (%)	t (%)
1	330	0.05	2.5	20.10	1.47	3.37	9.19
2	330	0.15	2.0	20.10	1.47	3.46	10.33
3	280	0.05	2.5	20.10	1.54	3.61	10.23
4	280	0.05	2.0	20.10	1.54	2.98	10.18
5	330	0.05	2.5	19.98	1.47	5.03	18.10
6	280	0.15	2.5	20.10	1.47	3.16	10.58
7	330	0.15	2.0	20.10	1.54	3.14	8.77
8	280	0.15	2.5	19.98	1.54	4.97	17.79
9	280	0.05	2.0	19.98	1.47	4.86	15.62
10	330	0.15	2.5	19.98	1.54	4.47	15.88
11	280	0.15	2.0	19.98	1.47	4.97	14.66
12	330	0.05	2.0	19.98	1.54	4.87	15.80

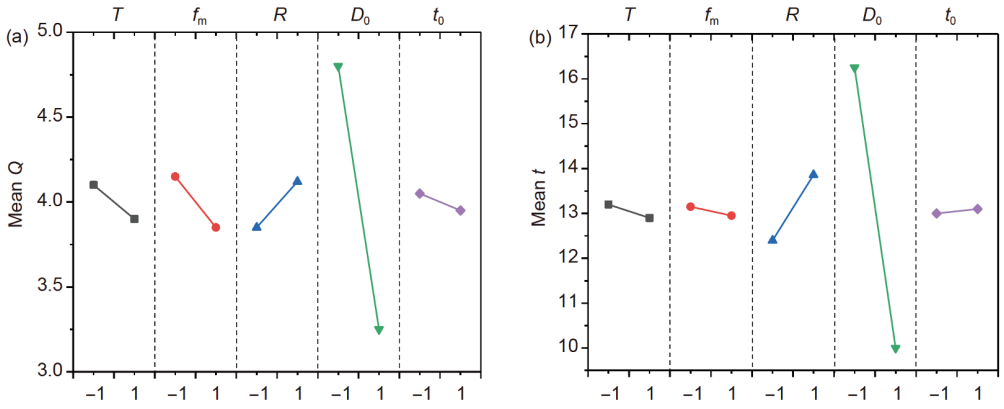

Figure 8 (Color online) Main effects of the uncertainty factors for the responses. (a) Q; (b) t.

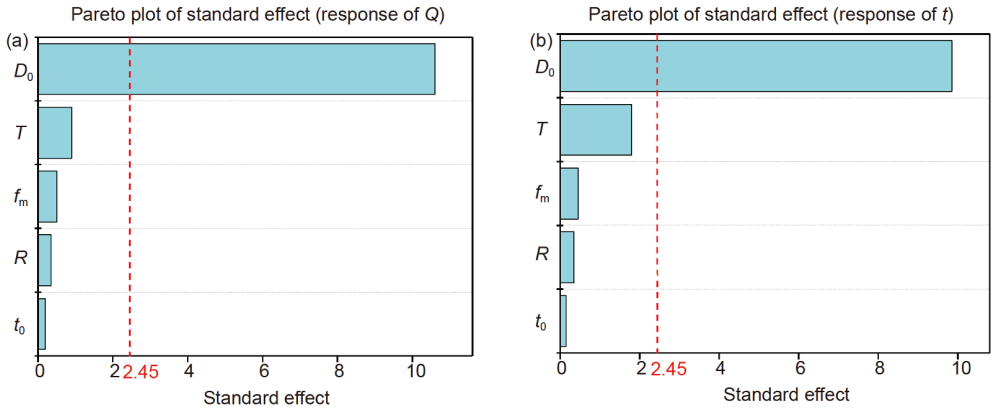

Figure 9 (Color online) Pareto plots of the standard effect of the uncertainty factors for the responses. (a) Q; (b) t.

Table 5 Cross array with control and uncontrolled factors

Control factors					Uncontrolled factors inner array			
					Z_1	1	…	3
					Z_2	2	…	2
					Z_3	3	…	2
	X_1	X_2	X_3	X_4				
Outer array	1	1	2	3		y_{11}	y_{12}	…	y_{1j}
	1	2	3	2		y_{21}	y_{22}	…	y_{2j}
	1	3	1	1		y_{31}	y_{32}	…	y_{3j}
	…	…	…	…		…	…	…	…
	1	1	2	2		y_{i1}	y_{i2}	…	y_{ij}

$$t^{\sigma} = 42477.10474 - 5147.94378d_{\mathrm{m}} + 0.10548e + 6.09455K_{\mathrm{vp}} + 155.94757d_{\mathrm{m}}^2. \quad (7)$$

The accuracy evaluation of the dual RSMs is shown in Table 8. R^2 is greater than 0.9, which implies that dual RSMs have high precision.

Based on the dual-RSM (eqs. (4) and (5)), the interactions between the mandrel diameter d_{m} and elongation e, have a significant impact on Q^{μ}, and the 3D interaction response surface is shown in Figure 10. When d_{m} is moderate and e is large, Q^{μ} is the minimum. When d_{m} remains unchanged and e increases, Q^{μ} decreases. When e remains unchanged and d_{m} increases, Q^{μ} first decreases and then increases, and the variation is large. Therefore, the impact of d_{m} on Q^{μ} is more significant than that of e on Q^{μ}.

Based on the dual-RSM (eqs. (4) and (5)), the interactions

Table 6 Cross array for response Q

Control factors				Uncertainty factors							Objectives	
				UD	1	2	3	4	5	6	Mean	SD
				T	280	290	300	310	320	330		
	d_m	e	K_{vp}	f_m	0.07	0.11	0.15	0.05	0.09	0.13	Q^{μ}	Q^{σ}
				R	2.2	2.5	2.1	2.4	2.0	2.3		
				D_0	20.10	20.076	20.052	20.028	20.004	19.98		
1	16.42	0	1.1		5.24	4.95	4.86	4.55	3.69	5.32	4.77	0.36
2	16.82	0	1.1		4.30	4.31	5.65	4.11	5.12	5.71	4.87	0.52
3	16.42	2	1.1		5.12	4.98	4.72	4.38	4.28	5.18	4.78	0.15
4	16.82	2	1.1		4.02	4.16	5.44	4.00	4.64	5.52	4.63	0.49
5	16.42	1	1.0		5.50	5.47	5.23	5.09	4.96	5.24	5.25	0.04
6	16.82	1	1.0		4.48	4.56	5.87	4.46	5.15	4.99	4.92	0.30
7	16.42	1	1.2		5.12	5.01	4.65	4.41	4.29	5.09	4.76	0.13
8	16.82	1	1.2		4.07	4.31	4.27	4.62	4.73	5.85	4.64	0.41
9	16.62	0	1.0		4.76	4.61	4.57	4.31	4.37	4.63	4.54	0.03
10	16.62	2	1.0		4.56	4.46	4.42	4.21	4.25	4.42	4.39	0.02
11	16.62	0	1.2		4.40	4.33	4.10	3.87	3.62	4.57	4.15	0.13
12	16.62	2	1.2		4.21	4.10	3.90	3.75	3.61	4.43	4.00	0.09
13	16.62	1	1.1		4.24	4.15	4.01	3.80	3.73	4.59	4.09	0.10
14	16.62	1	1.1		4.24	4.15	4.01	3.80	3.73	4.59	4.09	0.10
15	16.62	1	1.1		4.24	4.15	4.01	3.80	3.73	4.59	4.09	0.10
16	16.62	1	1.1		4.24	4.15	4.01	3.80	3.73	4.59	4.09	0.10
17	16.62	1	1.1		4.24	4.15	4.01	3.80	3.73	4.59	4.09	0.10

Table 7 Cross array for response t

Control factors				Uncertainty factors							Objectives	
				UD	1	2	3	4	5	6	Mean	SD
				T	280	290	300	310	320	330		
	d_m	e	K_{vp}	f_m	0.07	0.11	0.15	0.05	0.09	0.13	t^{μ}	t^{σ}
				R	2.2	2.5	2.1	2.4	2	2.3		
				D_0	20.10	20.076	20.052	20.028	20.004	19.98		
1	16.42	0	1.1		10.00	8.66	9.12	8.86	10.34	11.24	9.70	1.00
2	16.82	0	1.1		10.58	10.58	18.46	11.97	18.34	18.6	14.76	16.80
3	16.42	2	1.1		9.73	9.07	9.33	8.62	9.25	11.17	9.53	0.78
4	16.82	2	1.1		10.13	10.40	17.28	11.30	18.29	18.40	14.30	16.64
5	16.42	1	1.0		10.81	9.75	10.13	10.13	10.94	11.24	10.50	0.33
6	16.82	1	1.0		11.32	10.77	17.32	11.66	18.26	16.97	14.38	12.04
7	16.42	1	1.2		9.82	9.04	9.40	9.00	9.45	11.24	9.66	0.69
8	16.82	1	1.2		10.90	10.07	11.16	9.00	16.92	18.05	12.68	14.53
9	16.62	0	1.0		11.75	11.08	12.36	11.16	12.39	12.95	11.95	0.56
10	16.62	2	1.0		11.49	10.63	12.51	10.70	12.44	12.92	11.78	0.97
11	16.62	0	1.2		10.29	9.50	10.57	8.98	10.09	12.39	10.30	1.37
12	16.62	2	1.2		9.76	8.72	8.80	9.84	9.83	12.78	9.96	2.18
13	16.62	1	1.1		10.10	9.56	9.26	9.01	10.86	12.71	10.25	1.89
14	16.62	1	1.1		10.10	9.56	9.26	9.01	10.86	12.71	10.25	1.89
15	16.62	1	1.1		10.10	9.56	9.26	9.01	10.86	12.71	10.25	1.89
16	16.62	1	1.1		10.10	9.56	9.26	9.01	10.86	12.71	10.25	1.89
17	16.62	1	1.1		10.10	9.56	9.26	9.01	10.86	12.71	10.25	1.89

between d_m and the booster coefficient K_{vp} have a significant impact on t^{μ}, and the 3D interaction response surface is shown in Figure 11. When d_m is small and K_{vp} is large, t^{μ} is the minimum. When d_m remains unchanged and K_{vp} increases, t^{μ} decreases. When K_{vp} remains unchanged and d_m increases, t^{μ} increases, and its variation is large. The impact of d_m on t^{μ} is more significant than that of K_{vp}.

4.3 Optimization analysis and experimental verification

As shown in Figure 12, the black region is a feasible solution. In general, the multiobjective optimization solution is not unique; rather, it has a group of solutions, called the Pareto optimal set (the red circle in Figure 12). Any solution in this set is better than other viable solutions. However, in the Pareto optimal sets, mutual constraints and conflicts are present among various targets, rendering the solution of multiobjective optimization unable to achieve the optimal solution of a single target simultaneously (blue solid circle in Figure 12). Thus, simultaneously minimizing the cross-section distortion rate and the wall-thickness thinning rate is difficult. Therefore, the minimum distance method is adopted to select the optimal solution from the Pareto optimal set. It not only ensures the minimum tube cross-section distortion but also reduces the outside wall-thickness thinning of the tube.

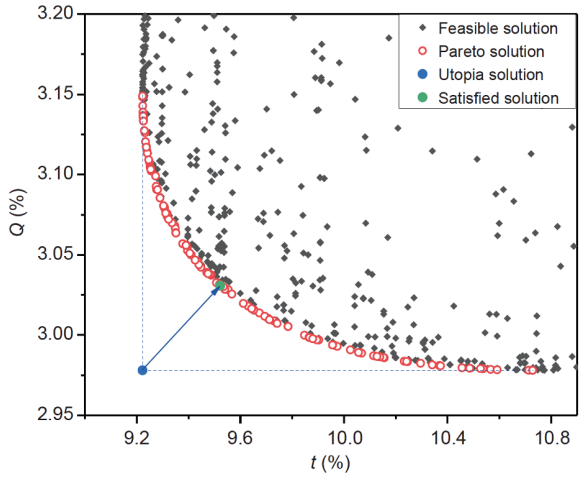

Figure 12 Solution set of the forming parameters by NSGA-II.

Table 8 Accuracy evaluation of the dual RSMs

	Q^{μ}	Q^{σ}	t^{μ}	t^{σ}
R^2	0.9853	0.9876	0.9488	0.9757
Adjust R^2	0.9765	0.9780	0.9181	0.9675

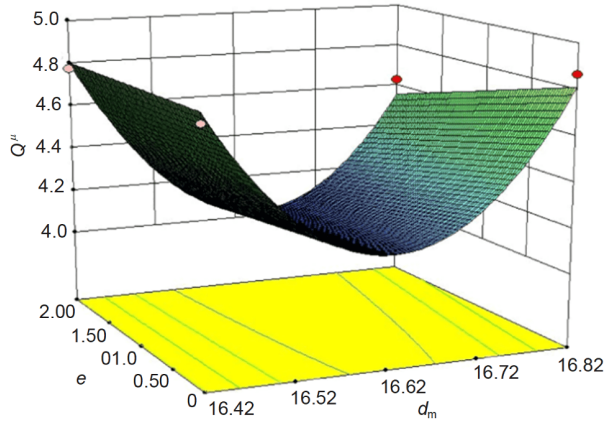

Figure 10 3D response surface. Effect of mandrel diameter d_m and mandrel elongation e on Q^{μ}.

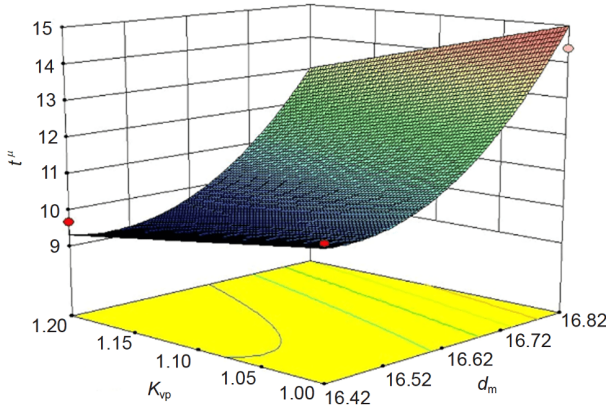

Figure 11 3D response surface. Effect of mandrel diameter d_m and boost coefficient K_{vp} on t^{μ}.

The minimum distance method can be expressed as follows:

$$\text{Minimum } D = \sqrt{\sum_{\tau=1}^{U}(f_{\tau} - f_{\tau}^{\text{utopia}})^2}, \tag{8}$$

where U represents the number of targets, τ is the single solution of the Pareto optimal set, and f_{τ}^{utopia} is the optimal solution that considers only the single target.

Based on this method, the final optimal solution was determined (green solid circle in Figure 12), and Q and t are 3.03% and 9.52%, respectively. The optimal combination of the forming parameters is d_m=16.60 mm, K_{vp}=1.20, and e=1.90 mm. Figure 13 shows the simulated result with and without optimization for the bending of $\Phi\times t\times R$ (20 mm×1.5 mm×30 mm) HSTT. After optimization, the cross-section distortion is reduced and wall-thickness distribution becomes more uniform. The obtained results are listed in Table 9. Comparing the forming results with and without optimization, we found that with the process of multiobjective robust optimization, Q decreases by 38.1% compared with that obtained without optimization, and t decreases by 27.8%.

To verify the effectiveness and reliability of the multiobjective RDO method based on the NSGA-II genetic al-

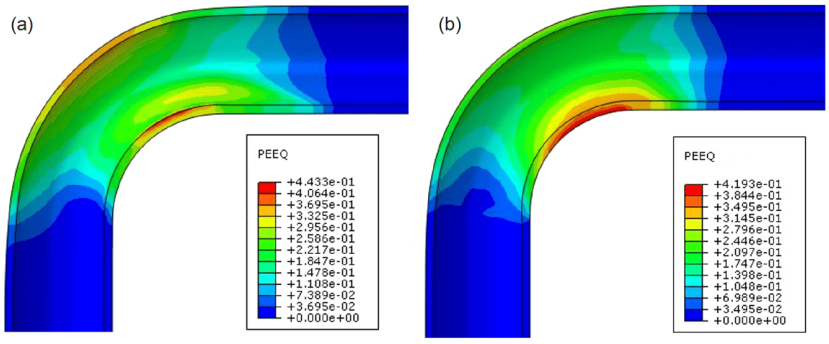

Figure 13 (Color online) Forming result under different conditions. (a) Without optimization; (b) robust optimization.

Table 9 Comparison of forming results under different conditions

	d_m (mm)	e (mm)	K_{vp}	Q (%)	t (%)
Robust optimization	16.60	1.19	1.20	3.10	9.80
Without optimization	16.62	0	1.0	5.01	13.58

gorithm for the optimization of the NC-HRDB process, the forming parameters of the same RDO were selected, and the NC-HRDB of HSTT was repeated several times. The heating temperature was 300°C. After 10 min of heating, the bending test was conducted five times, and the formed tubes are shown in Figure 14. The average maximum cross-section distortion rate, variance, and fluctuation of the five elbows are 3.15%, 0.0017, and 2.54%, respectively. The maximum thickness reduction rate is 10.82%.

5 Conclusions

Facing the challenge of the NC-HRDB forming of HSTT with small bending radii for tube systems and combining with RDO and FE numerical simulation, we investigated a numerical model of NC-HRDB, the significance analysis of uncertainty factors, and the RDO of forming parameters. The conclusions are as follows.

(1) The analysis for the significance of uncertainty factors on HRDB was performed using an orthogonal experimental design, and the significant factors among the uncertainty factors were obtained.

(2) Using the Taguchi inner and outer arrays, establishing the dual-RSM, maximum section distortion, and maximum wall-thickness thinning, the robust optimization designs of the uncertainty factors could be achieved.

(3) Based on the NSGA-II algorithm and minimum distance selection method, the final robust solution is obtained: d_m=16.60 mm, e=1.19 mm, and K_{vp}=1.20. The results show that the RDO of the forming parameters can effectively reduce the section distortion and wall-thickness thinning caused by the fluctuation in the uncertainty factors and also improve the stability of the two objectives.

This work was supported by the National Natural Science Foundation of China (Grant No. 51775441).

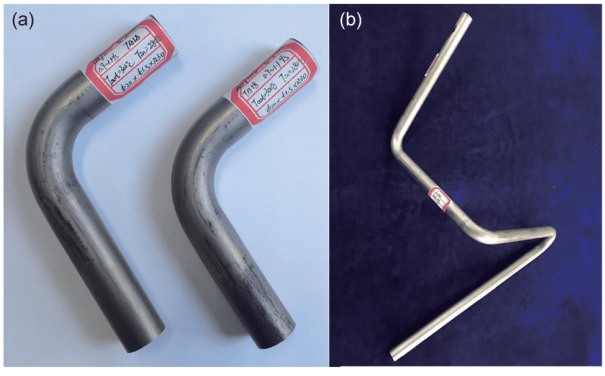

Figure 14 (Color online) Warm bending experiment verification of HSTT based on robust design. (a) Single-bend tubes; (b) multibend tubes.

1 Yang H, Li H, Ma J, et al. Temperature dependent evolution of anisotropy and asymmetry of α-Ti in thermomechanical working: Characterization and modeling. Int J Plast, 2020, 127: 102650
2 Li H, Yang H, Xu J, et al. Knowledge-based substep deterministic optimization of large diameter thin-walled Al-alloy tube bending. Int J Adv Manuf Technol, 2013, 68: 1989–2004
3 Hao N, Li L. An analytical model for laser tube bending. Appl Surf Sci, 2003, 208-209: 432–436
4 Guan Y, Yuan G, Sun S, et al. Process simulation and optimization of laser tube bending. Int J Adv Manuf Technol, 2013, 65: 333–342
5 Hu Z. Elasto-plastic solutions for spring-back angle of pipe bending using local induction heating. J Mater Processing Tech, 2000, 102: 103–108
6 Collie G J, Higgins R J, Black I. Modelling and predicting the deformed geometry of thick-walled pipes subjected to induction bending. Proc Inst Mech Eng Part L J Mater Des Appl, 2010, 224: 177–189

7 Huang L, Lu X. Technology analysis of hot pushing pipe bending and horn mandrel design. In: Proceedings of International Conference on Mechanical Engineering and Intelligent Systems. Yinchuan, 2015. 842–845
8 Tao Z, Li H, Ma J, et al. FE modeling of a complete warm-bending process for optimal design of heating stages for the forming of large-diameter thin-walled Ti-6Al-4V tubes. Manufacturing Rev, 2017, 4: 8–24
9 Simonetto E, Venturato G, Ghiotti A, et al. Modelling of hot rotary draw bending for thin-walled titanium alloy tubes. Int J Mech Sci, 2018, 148: 698–706
10 Zhang Z, Yang H, Li H, et al. Thermo-mechanical coupled 3D-FE modeling of heat rotary draw bending for large-diameter thin-walled CP-Ti tube. Int J Adv Manuf Technol, 2014, 72: 1187–1203
11 Li H, Yang J, Chen G, et al. Towards intelligent design optimization: Progress and challenge of design optimization theories and technologies for plastic forming. Chin J Aeronautics, 2021, 34: 104–123
12 Ou H, Wang P, Lu B, et al. Finite element modelling and optimisation of net-shape metal forming processes with uncertainties. Comput Struct, 2012, 90-91: 13–27
13 Huang T, Song X, Liu X. The multi-objective robust optimization of the loading path in the T-shape tube hydroforming based on dual response surface model. Int J Adv Manuf Technol, 2016, 82: 1595–1605
14 Chen X W, Liu Z H, Zhang J L. Robust optimization for tube bending process based on finite element method. Key Eng Mater, 2012, 531-532: 746–750
15 Strano M. Optimization under uncertainty of sheet-metal-forming processes by the finite element method. Proc Institution Mech Engineers Part B-J Eng Manufacture, 2006, 220: 1305–1315
16 Sun G, Li G, Gong Z, et al. Multiobjective robust optimization method for drawbead design in sheet metal forming. Mater Des, 2010, 31: 1917–1929
17 Yin H, Fang H, Xiao Y, et al. Multi-objective robust optimization of foam-filled tapered multi-cell thin-walled structures. Struct Multidisc Optim, 2015, 52: 1051–1067
18 Li H, Xu J, Yang H, et al. Sequential multi-objective optimization of thin-walled aluminum alloy tube bending under various uncertainties. Trans Nonferrous Met Soc China, 2017, 27: 608–615